

Alma Mater Studiorum Università di Bologna
Archivio istituzionale della ricerca

Benchmarking dispersion-corrected DFT methods for the evaluation of materials with anisotropic properties: Structural, electronic, dielectric, optical and vibrational analysis of calcite (CaCO₃, space group: R 3 c)

This is the final peer-reviewed author's accepted manuscript (postprint) of the following publication:

Published Version:

Ulian G., Moro D., Valdrè Giovanni (2021). Benchmarking dispersion-corrected DFT methods for the evaluation of materials with anisotropic properties: Structural, electronic, dielectric, optical and vibrational analysis of calcite (CaCO₃, space group: R 3 c). PHYSICAL CHEMISTRY CHEMICAL PHYSICS, 23(34), 18899-18907 [10.1039/d1cp02673a].

Availability:

This version is available at: <https://hdl.handle.net/11585/844561> since: 2024-02-13

Published:

DOI: <http://doi.org/10.1039/d1cp02673a>

Terms of use:

Some rights reserved. The terms and conditions for the reuse of this version of the manuscript are specified in the publishing policy. For all terms of use and more information see the publisher's website.

This item was downloaded from IRIS Università di Bologna (<https://cris.unibo.it/>).
When citing, please refer to the published version.

(Article begins on next page)

ARTICLE

Benchmarking dispersion-corrected DFT methods for the evaluation of materials with anisotropic properties: structural, electronic, dielectric, optical and vibrational analysis of calcite (CaCO_3 , space group $R\bar{3}c$)

Received 00th January 20xx,
Accepted 00th January 20xx

DOI: 10.1039/x0xx00000x

Gianfranco Ulian,^{*a} Daniele Moro^a and Giovanni Valdrè^{*a}

Calcite (CaCO_3 , space group $R\bar{3}c$) is a solid phase whose well-known highly anisotropic physical properties can be exploited to compare and calibrate various theoretical simulation methods. In this work, to benchmark different *ab initio* Density Functional Theory approaches that include for the first time corrections for dispersive forces, a systematic analysis of structural, electronic, dielectric, optical and vibrational properties of calcite is performed. The simulations considered the generalized-gradient approximation functional PBE and the hybrid B3LYP and PBE0, whereas the DFT-D2 and DFT-D3 schemes were adopted to account for the long-range interactions. This study suggests an overall better agreement between the theoretical results obtained with the DFT functionals corrected for the dispersive forces, with a better performance of hybrid functionals over PBE.

1. Introduction

Calcite (space group $R\bar{3}c$, trigonal crystal system) is the polymorph of calcium carbonate that is stable at ambient conditions.^{1,2} It is commonly represented with its trigonal lattice ($a = b \neq c$, $\alpha = \beta = 90^\circ$, $\gamma = 120^\circ$), which contains six formula units ($Z = 6$) of CaCO_3 , but the primitive cell identified by X-ray diffraction (XRD) is rhombohedral, with $a = b = c$ and $\alpha = \beta = \gamma \approx 46^\circ$ and $Z = 2$.³ Internally, calcite is made from alternatively stacked layers of Ca^{2+} ions and CO_3^{2-} anions, with each cation coordinating six oxygen atoms from six different carbonate groups (octahedral coordination). A graphical representation of the hexagonal and rhombohedral unit cells of calcite are presented in Figure 1.

It is well-known that calcite is a highly birefringent material, with the difference between the ordinary (n_o) and extraordinary (n_e) refractive indexes being $n_o - n_e = \delta = 0.172$. This property originates from the crystal chemistry of the mineral and the peculiar configuration of the carbonate ions in the crystal, as the carbonate ions are more polarizable by an electric field that oscillates parallel to the anionic plane than by orthogonal to it. The transparent variety of calcite known as “Iceland spar” has been widely employed in optical microscopes as polarizing (Nicol) prism, before being substituted by other types of polarizers. This property is exploited not only by chemists, mineralogists, petrologists and materials scientists, but also in

other fields, such as optical and instrumentation engineering. In fact, transparent calcite is employed in small fragments as a standard material to study the optical alignment and spinning of microscopic particles trapped by elliptically polarized laser beams (optical tweezers).^{4,5} Briefly, if there is a change in the angular momentum carried by the light, there will be a corresponding torque on the material,⁶ which could be employed, to cite an example, to build optically-driven microscopic machines.⁴

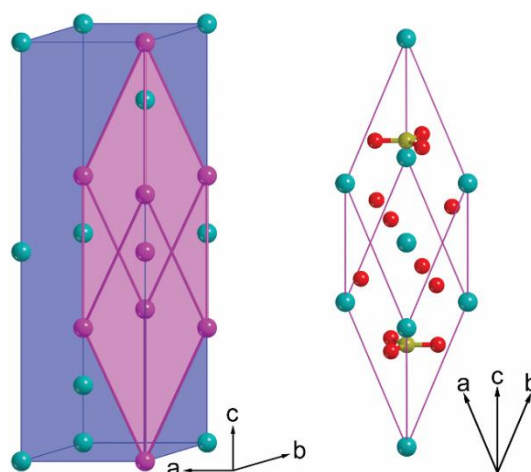


Fig. 1 Ball-and-stick representation of the calcite structure. In the left panel, the relationship between the trigonal crystallographic cell of calcite (in blue) and the primitive, rhombohedral cell (in purple) is shown. The right panel reports the internal geometry of the rhombohedral unit cell of CaCO_3 . Calcium, carbon and oxygen atoms are coloured in cyan, ochre and red, respectively.

^a Centro di Ricerca Interdisciplinare di Biomineralogia, Cristallografia e Biomateriali, Dipartimento di Scienze Biologiche, Geologiche e Ambientali, Università di Bologna “Alma Mater Studiorum”, Piazza di Porta San Donato 1, 40126 Bologna, Italy. E-mail: giovanni.valdre@unibo.it

Thanks to the extensive experimental knowledge of its various properties, calcite can be viewed as a prototypical material to study, develop and calibrate theoretical methods down to atomic scale, which could be furtherly employed for other, less-known materials. In fact, atomic-scale simulations provide an invaluable tool to both increase the understanding of the material properties at (sub-)nanometre level and to model and predict the behaviour of new materials.

Atomistic simulations of calcite are not new to the field, as both force field (classical mechanics) and *ab initio* quantum mechanics simulations were performed in the past.^{7–11} The present work is intended to address some specific issues and discrepancy on calcite CaCO₃. One of them is the larger *c* lattice parameter obtained at *ab initio* level found in literature^{10, 11} with respect to the experimental X-ray diffraction (XRD) refinements.^{3, 12} The authors' of the present paper suppose that this discrepancy could be due to a well-known limitation of Density Functional Theory (DFT) methods in describing long-range interactions, which could play a role in determining the structural properties of calcite. This is not a trivial matter, since the correct determination of lattice parameters and internal geometry are of utmost importance for modelling other properties, such as electronic, dielectric, optical and vibrational ones. For this reason, it is here proposed to characterize the calcite structure including for the first time the contributions of dispersive forces in the calculation of the total energy of the system. Then, electronic, dielectric, optical and vibrational properties were calculated.

The present paper is organized as follows. The next section (2) is devoted to a brief, but exhaustive and necessary introduction to the simulation methods within the Density Functional Theory. Section 3 reports the results obtained with the proposed approaches, together with a detailed discussion of the data against both experimental and theoretical literature on calcite. Finally, section 4 draws the summary and conclusions of the present work.

2. Computational Details

A. Hamiltonian and computational parameters

The results obtained in the present work were obtained through *ab initio* simulations carried out with the CRYSTAL17 code, which employs the Hartree–Fock and Kohn–Sham, self-consistent field (SCF) method for the investigation of periodic systems.¹³

Three well-known Density Functional Theory (DFT) functionals were selected to perform all the simulations reported in the present work. The first one is the generalized-gradient approximation (GGA) formulation developed by Perdew–Burke–Ernzerhof (PBE), which is a non-empirical DFT functional.¹⁴ The second and third functionals are the hybrid B3LYP^{15–17} and PBE0,¹⁸ which include 20% and 25% of Hartree–Fock energy contributions to the DFT exchange term, respectively.

The calculation of the total energy of periodic system was performed on a pruned grid of 75 radial and 974 angular points, generated through the Gauss–Legendre and Lebedev quadrature

schemes. The same grid was employed in previous works on calcite with the CRYSTAL code.^{10, 11} The thresholds controlling the accuracy of the calculation of the Coulomb and exchange integrals (ITOL1 to ITOL5 keywords in CRYSTAL) have been set to ITOL1 – ITOL4 = 8 and ITOL5 = 16, meaning that when the overlap between two atomic orbitals is lower than 10^{−ITOL}, the corresponding integral is either discarded or treated with less precision, as explained by Dovesi and collaborators.¹³ The Hamiltonian matrix has been diagonalized through the Monkhorst and Pack scheme,¹⁹ using a 6×6×6 *k*-mesh with 32 *k*-points.

B. Inclusion of long-range interactions

As cited in the Introduction, a well-known limitation of both GGA and hybrid Density Functional Theory functionals is the improper treatment of long-range interactions, with several drawbacks in the description of structural, vibrational, mechanical and other properties. The most common approach to overcome this issue is including an additional energy term (*E*_{vdw}) to the DFT energy (*E*_{DFT}), hence the total energy of the system is *E*_{TOT} = *E*_{DFT} + *E*_{vdw}. The van der Waals energy is thus added in *a posteriori* fashion and, in the present work, the DFT-D2 and DFT-D3 formulations proposed by Grimme and collaborators were employed.^{20, 21} Very briefly, these corrections are expressed as:

$$E_{\text{DFT-D2}} = -\frac{1}{2} \sum_{i=1}^N \sum_{j=1}^N \sum_{\mathbf{g}} \frac{C_{6ij}}{r_{ij,\mathbf{g}}^6} f_{\text{dump},6}(r_{ij,\mathbf{g}})$$

and

$$E_{\text{DFT-D3}} = -\frac{1}{2} \sum_{i=1}^N \sum_{j=1}^N \sum_{\mathbf{g}} \left[\frac{C_{6ij}}{r_{ij,\mathbf{g}}^6} f_{\text{dump},6}(r_{ij,\mathbf{g}}) + \frac{C_{8ij}}{r_{ij,\mathbf{g}}^8} f_{\text{dump},8}(r_{ij,\mathbf{g}}) \right]$$

where the summations run over the number of atoms *N*, *r*_{*ij*,*g*} is the internuclear distance between atom *i* in cell *g* = 0 (reference cell) and atom *j* in cell *g*, *C*_{6*ij*} and *C*_{8*ij*} are the *n*th-order dispersion coefficients for atom pairs *ij* and *f*_{dump,*n*}(*r*_{*ij*,*g*}) is a damping function that suppresses the correction for long-range interactions for short distances, where other bonds (*e.g.* covalent) play the relevant role. In the DFT-D2 scheme, the damping function has the following expression:

$$f_{\text{dump},6}(r_{ij,\mathbf{g}}) = s_6 \left[1 + e^{-d(r_{ij,\mathbf{g}}/R_{\text{vdw}}-1)} \right]^{-1}$$

where *s*₆ is a scaling parameter optimized for different functionals (*e.g.*, *s*₆ = 0.75 for PBE) and *R*_{vdw} is the sum of van der Waals radii of atoms *i* and *j* and *d* is a factor that sets the steepness of the damping function (*d* = 20). Also, the *C*_{6*ij*} parameters are calculated as a geometrical mean:

$$C_{6ij} = \sqrt{C_{6i}C_{6j}}$$

where *C*_{6*i*} and *C*_{6*j*} are tabulated for each atom.²⁰ Conversely, in the DFT-D3 scheme the *C*_{*nij*} (*n* = 6, 8) parameters are dependent on the geometry of the system, and not fixed as in the DFT-D2

correction.²² The damping function here adopted is the one proposed by Becke and Johnson:^{23–25}

$$f_{\text{damp},n}(r_{ij},g) = \frac{s_n r_{ij}^n}{r_{ij}^n + f(R_{0ij})^n}$$

with $R_{0ij} = \sqrt{C_{8ij}/C_{6ij}}$ and $f(R_{0ij}) = \alpha_1 R_{0ij} + \alpha_2$. In this formulation, $s_6 = 1$, s_8 , α_1 and α_2 are adjustable parameters. For a detailed explanation of the DFT-Dn ($n = 2, 3$) corrections, the reader can refer to the works of Grimme and collaborators.^{20, 22}

C. Basis sets

The multielectronic wave function is constructed as an antisymmetrized product (Slater determinant) of mono-electronic crystalline orbitals (CO) that are linear combinations of atomic orbitals (AOs) centred on each atom of the crystal (LCAO approach). In turn, AOs are linear combinations of Gaussian-type functions (GTF, the product of a Gaussian times a real solid spherical harmonic to give s-, p- and d-type AOs). The basis sets here employed are 8-6511(21), 6-311(11) and 8-411(11) for calcium, carbon and oxygen, respectively, taken from the works of Valenzano and co-workers for the same mineral phase (basis set labelled as BSD),^{11, 26} and also extended to other solid systems, such as hydroxylapatite^{27–29} and phyllosilicates.^{30–32}

D. Geometry optimization and simulation of vibrational and dielectric properties

The geometry optimization procedure, encompassing at the same time variations of lattice vectors and internal coordinates, was performed with an analytical gradient method for the atomic positions and a numerical gradient for the unit cell parameters. To ensure well-converged structures for electronic, dielectric, optical and vibrational properties, the optimization procedure ended when the gradient and the maximum atomic displacement were lower than 10^{-5} hartree bohr⁻¹ and $4 \cdot 10^{-5}$ bohr, respectively, with respect to the previous optimization step.

In periodic systems and within the harmonic approximation, the vibrational frequencies at Γ point are evaluated diagonalising the central zone ($\mathbf{k} = 0$) mass-weighted Hessian matrix. In CRYSTAL17, the calculation of the Hessian at equilibrium is made by the analytical evaluation of the energy first derivatives with respect to the atomic displacements, while second derivatives at equilibrium (where all first derivatives are zero) are calculated numerically using a "two-point" formula. More details on the vibrational calculation made by CRYSTAL can be found in dedicated literature.³³ Furthermore, the effect of the longitudinal optical (LO) and transverse optical (TO) splitting in the phonon dispersion was taken into account.³⁴ The LO-TO splitting is an effect of long-range Coulomb fields arising from the coherent displacement of the atom nuclei, which is neglected in standard calculations within the harmonic approximation because of the imposed periodic boundary conditions. The calculation of such splitting (non-analytical contribution) depends on the electronic (clamped nuclei) dielectric tensor ϵ_0 and on the Born effective charge tensor associated with each atom. Both quantities were obtained through a coupled-perturbed Kohn-Sham (CPKS) approach. Specific details on the

calculation of the dielectric tensor can be found in the work of Maschio et al.,³⁵ whereas the analytical evaluation of the Born charge tensor in the works of Pascale *et al.*³³ and Maschio and co-workers.^{36, 37} For the calculation of the dielectric tensor, the unit cell of calcite was oriented with the **a**- and **c**-axes parallel to the $-x$ and z Cartesian directions, respectively.

3. Results and discussion

A. Crystal structure

Briefly, it should be recalled that calcite presents a mixed bonding scheme comprising both covalent (C – O) and ionic ($\text{Ca}^{2+} \cdots \text{O}^{2-}$) interactions. The former acts mainly along the **a** = **b** crystallographic axes, while ionic bonds hold together the calcium and carbonate ion layers along the [001] direction.

Table 1 reports all the results of the geometry optimization of calcite conducted in the present paper with different Density Functional Theory Hamiltonians, also corrected for long-range interactions. The experimental unit cell refinements of calcite performed by Maslen and collaborators¹² and by Redfern and Angel³⁸ are also reported for the sake of a comparison. The XRD results are very similar, with a volume difference of less than 0.1%. In the following, the results of Maslen et al.¹² will be used for discussing the present theoretical results, for reasons of completeness.

Differences in the calculated structural properties with respect to the X-ray diffraction unit cell refinement are shown as a bar plot in Figure 2. Both uncorrected GGA (PBE) and hybrid (B3LYP and PBE0) DFT functionals properly describe the covalent bonds within the CO_3^{2-} ions, since the $a = b$ lattice parameters are overestimated by +1.1%, +1.0% and +0.3% by PBE, B3LYP and PBE0, respectively, with respect to the experimental data.¹² The same applies to the C – O distances ($d_{\text{C-O}}$), which are slightly overestimated by about +1.1% and 0.3% by PBE and B3LYP, whereas at PBE0 level the bonds are underestimated by –0.1%. However, each selected functional overestimates the c lattice parameter between 0.9% (PBE0) and 1.5% (B3LYP and PBE), with an overall expansion of the unit cell in the range 1.5–3.7% depending on the functional.

Table 1. Unit cell parameters a and c (in Å) and volume V (in Å³), c/a ratio and C – O and Ca \cdots O distances ($d_{\text{C-O}}$ and $d_{\text{Ca-O}}$, respectively, in Å) of calcite CaCO_3 , calculated with different Density Functional Theory methods. Experimental XRD data are also reported for a comparison.

Method	a	c	V	c/a	$d_{\text{C-O}}$	$d_{\text{Ca-O}}$
PBE	5.045	17.313	381.67	3.432	1.2976	2.3882
PBE-D2	5.020	16.955	370.08	3.377	1.2952	2.3607
PBE-D3	5.026	17.034	372.64	3.389	1.2958	2.3668
B3LYP	5.041	17.320	381.08	3.436	1.2879	2.3915
B3LYP-D*	5.028	16.968	371.52	3.375	1.2860	2.3695
B3LYP-D3	5.007	16.822	365.17	3.360	1.2846	2.3535
PBE0	5.007	17.215	373.73	3.438	1.2824	2.3745
PBE0-D2	4.984	16.849	362.42	3.381	1.2801	2.3472
PBE0-D3	4.988	16.932	364.85	3.395	1.2806	2.3530
XRD ¹²	4.991	17.062	368.1	3.419	1.2840	2.3590
XRD ³⁸	4.9891	17.0610	367.787	3.420	-	-

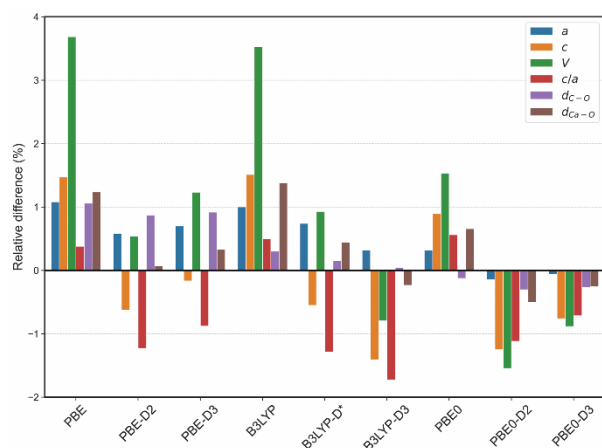


Fig. 2 Relative difference (in %) between calcite lattice parameters a and c , unit cell volume V , c/a ratio and C – O and Ca – O distances calculated with different DFT approaches and those obtained by X-ray diffraction data.¹²

These observations are in line with those reported by Valenzano and co-workers for the PBE and B3LYP Hamiltonians.¹¹ The results suggest this expansion effect could be due to the poor description of the ionic $\text{Ca}^{2+} \cdots \text{O}^{2-}$ interactions, as they are overestimated by +1.2%, +1.4% and 0.7% employing PBE, B3LYP and PBE0 functionals, respectively.

In addition, since the simulations are conducted without thermal effects (*i.e.*, they are referred to 0 K), one should expect that the theoretical unit cell be with smaller volumes than the experimental one, which was measured at room conditions (ca. 298 K).

By adding the *a posteriori* contribution of weak dispersive interactions, both lattice and internal geometries of calcite are more in line with the X-ray diffraction data. With respect to the non-corrected functionals, the DFT-D2 scheme caused a contraction of the unit cell volume of about 3.0% when used in conjunction with the PBE and PBE0 functionals, and the specifically parametrized B3LYP-D* approach shrank the unit cell volume by about 2.5%. In each approach, the c lattice parameter was smaller than that experimentally measured, whereas the a -axis parameter was still larger but for the PBE0-D2 method. The less empirical DFT-D3 approach^{21, 22} provided more compacted unit cell with respect to the DFT-D2 method when used with the hybrid B3LYP functional, whereas a small expansion by about 2.4 \AA^3 was observed for both PBE and PBE0 Hamiltonians. For PBE-D3, the unit cell volume was overestimated by just +1% with respect to the experimental findings, whereas both B3LYP-D3 and PBE0-D3 resulted in an underestimated V (−0.8% and −0.9%, respectively). For all the dispersion-corrected functionals, the c/a ratio is underestimated by about 1% due to the greater reduction of the c -axis length with respect to that of the a lattice parameter.

Considering the internal geometry, covalent C – O bond lengths and ionic $\text{Ca}^{2+} \cdots \text{O}^{2-}$ interactions are well described by dispersion-corrected hybrid B3LYP, with deviations as small as +0.05% and −0.23% with B3LYP-D3 approach, respectively. A systematic underestimation of about −0.25% of both atomic distances was observed when using the hybrid PBE0-D3 approach. Conversely, PBE-D3 showed an overestimation of

about +0.9% and +0.3% for C – O bonds and $\text{Ca}^{2+} \cdots \text{O}^{2-}$ interactions, respectively.

The present geometrical results are a first indication, as expected, of the importance of the inclusion of van der Waals interactions to the total energy, and hence to the structural features of the mineral phase. It is then expected a deep influence on other properties (*e.g.*, vibrational and mechanical) depending on the employed correction for the long-range interactions.

B. Electronic band gap, dielectric and optical properties

The electronic band structure of calcite was calculated along high-symmetry lines in the First Brillouin Zone (IBZ) of the rhombohedral unit cell, following the path $\Gamma\text{--}A\text{--}H\text{--}K\text{--}\Gamma\text{--}M\text{--}L\text{--}H$. A graphical representation of the band structure calculated with DFT Hamiltonians PBE, B3LYP and PBE0 is reported in Figure S1 in the Supplementary Materials. The band gaps calculated with the different functionals, also corrected for dispersive forces, are reported in Table 2.

Calcite is a well-known insulator, with an indirect band gap experimentally measured as $E_g = 6.0 \pm 0.35 \text{ eV}$ along $\Gamma \rightarrow M$.³⁹ The present data agree with the experimental evidence, but the absolute values show some differences. In particular, the PBE functional produced a smaller band gap ($E_g = 5.15 \text{ eV}$) because of the known limitations of GGA functionals in describing this electronic feature. Conversely, as expected, since B3LYP and PBE0 contain 20% and 25% of Hartree-Fock exchange, respectively, which commonly increases the band gap, the results from the hybrid functionals are larger than the experimental ones ($E_g = 7.42 \text{ eV}$ and $E_g = 8.01 \text{ eV}$ at B3LYP and PBE0 levels, respectively).

The inclusion of the van der Waals interactions is not incisive in determining variations in the band structure, because both DFT-D2 and DFT-D3 are *a posteriori* corrections. In fact, they affect the total energy of the system, but do not directly influence the generation/construction of the wavefunction, which is the quantity used to calculate the electronic bands.

Table 2. Static (ϵ_{xx}^0 and ϵ_{zz}^0) and high-frequency (ϵ_{xx}^∞ and ϵ_{zz}^∞) dielectric tensor components, ordinary (n_o) and extraordinary (n_e) refractive indexes (calculated at zero frequency), birefringence (δ) and band gap (E_g , eV) of calcite, simulated with different DFT methods and compared to experimental data.

Method	ϵ_{xx}^0	ϵ_{zz}^0	ϵ_{xx}^∞	ϵ_{zz}^∞	n_o	n_e	δ	E_g
PBE	9.43	7.14	2.76	2.17	1.660	1.474	0.187	5.15
PBE-D2	11.26	9.15	2.80	2.20	1.674	1.483	0.191	5.17
PBE-D3	9.96	7.76	2.79	2.19	1.671	1.481	0.190	5.17
B3LYP	7.96	6.35	2.55	2.06	1.598	1.434	0.164	7.42
B3LYP-D*	8.54	7.50	2.59	2.08	1.609	1.441	0.168	7.46
B3LYP-D3	8.32	7.36	2.61	2.09	1.616	1.447	0.169	7.48
PBE0	8.33	6.78	2.55	2.06	1.596	1.436	0.161	8.01
PBE0-D2	9.53	8.74	2.59	2.09	1.610	1.445	0.164	8.05
PBE0-D3	8.76	7.45	2.58	2.08	1.607	1.443	0.163	8.04
Experimental	8.5 ^a	8.0 ^a	2.7 ^a	2.2 ^a	1.640–1.660 ^b	1.486 ^b	0.1540–0.1740 ^b	6.0 ^c

^a Lide.⁴⁰ ^b Anthony and collaborators.⁴¹ ^c Baer and Blanchard.³⁹

The band gap calculated at GGA level is in agreement with the theoretical results of both Hossain et al.⁴² and Brik,⁴³ who calculated $E_g = 5.07 \text{ eV}$ and $E_g = 5.023 \text{ eV}$, respectively. However, in both works, where the CASTEP code was used, plane wave basis sets and the PBE functional were employed as

DFT framework. The small deviation between the cited results and the band gap calculated in the present work (5.15 eV at PBE level) is ascribable to differences in the basis set used (plane waves in the works of Hossain and collaborators⁴² and Brik,⁴³ versus Gaussian-type functions here) and other computational parameters (such as the k -point mesh).

Table 2 reports also the calculated static ϵ^0 and high-frequency ϵ^∞ dielectric tensor components along the xx and zz Cartesian directions, compared with experimental findings.⁴⁰ There is a substantial good agreement between the results here obtained with the hybrid functionals and the experimental tabulated data, with a non-null effect of the van der Waals corrections. In this sense, an overall better agreement is found with the B3LYP-D* approach. The ϵ_{zz}^0 term at both B3LYP and PBE0 levels, uncorrected for van der Waals interactions is underestimated by about 20%. Theoretical results obtained at the PBE level are also satisfactorily, with calculated data along the xx direction higher than the experimental ones by about 11 – 19%, depending on the type of correction for long-range interactions. However, it can be noted that PBE generally overestimates the static dielectric tensor components, especially when the DFT-D2 scheme is employed (+33%). In this case, the effect of dispersive forces is relevant, because the *a posteriori* corrections increase the interactions between the ions and, as a consequence, affect the polarizability of the solid phase.

Compared to the previous work of Valenzano and co-workers,¹¹ the results obtained for uncorrected B3LYP DFT functionals are almost identical. The same considerations can be extended to the refractive index, decomposed in the ordinary (n_o) and extraordinary (n_e) terms, and to the birefringence δ (see Table 2).

C. Vibrational properties

The thirty normal modes associated to the rhombohedral unit cell of calcite ($Z = 2$, $N = 10$ atoms, point group $\bar{3}m$) can be subdivided in the following irreducible representations (IRREPs):

$$\Gamma_{\text{tot}} = A_{1g} + 2A_{1u} + 3A_{2g} + 4A_{2u} + 4E_g + 6E_u$$

where the A_{2u} and E_u modes are active in infrared, the A_{1g} and E_g modes are active in Raman spectroscopy and the remaining A_{1u} and A_{2g} modes are silent. For the sake of clearness, A modes are singly degenerate (one associated atomic vibrational movement), whereas E modes are doubly degenerate (two vibrational modes having the same frequency). Of the total representation reported above, there are two representations ($A_{2u} + E_u = 3$ modes) related to translational of the atoms along the Cartesian directions, *i.e.* they are associated to acoustic vibrations of the solid, whereas the remaining 27 modes have a vibrational character. The results for the different combination of Hamiltonians and corrections for long-range interactions are reported in Table 3. Simulated infrared and Raman spectra of calcite are reported in Figure 3 and compared to experimental results.^{44, 45}

To estimate the quality of the calculated vibrational frequencies, with respect to the experimental findings, the minimum (Δ_{min}) and maximum (Δ_{max}) deviations, the mean deviation (MD) and

the mean absolute deviation (MAD) were calculated, according to the following expressions:¹¹

$$\Delta_{\text{max}} = \max(v_i - v_i^{\text{exp}})$$

$$\Delta_{\text{min}} = \min(v_i - v_i^{\text{exp}})$$

$$MD = \frac{1}{M} \sum_{i=1}^M v_i - v_i^{\text{exp}}$$

$$MAD = \frac{1}{M} \sum_{i=1}^M |v_i - v_i^{\text{exp}}|$$

In these formulas, the summation is limited to the number of active modes M , as it is not possible to calculate the deviations for silent modes.

Valenzano and co-workers¹¹ calculated the vibrational modes of calcite at PBE and B3LYP, without any correction for long-range interactions. The harmonic approximation results reported in the present work are in very good agreement with the cited ones, with small differences up to about 5 cm^{-1} because of the stricter convergence criteria imposed to the geometry optimization procedures and other computational parameters (*e.g.*, the truncation of the bielectronic integrals). It is worth noting that, with respect to the work of Valenzano and co-workers,¹¹ the computational settings here adopted allowed the reduction of the mean absolute deviation of B3LYP and PBE from 8.5 cm^{-1} to 7.6 cm^{-1} and from 26.4 cm^{-1} to 22.7 cm^{-1} , respectively.

As also reported in previous works,^{10, 11, 46} hybrid functionals usually perform better than standard GGA ones, and the present results further confirm this general trend. In fact, while PBE underestimates the vibrational frequencies, the B3LYP and PBE0 ones are closer to the experimental findings. Also, the calculated MAD of PBE0 is 14.7 cm^{-1} , a value between those of the pure GGA approach and of B3LYP. This result is in line with previous observations showing that the latter functional generally provides a better description of the vibrational properties of crystalline solids.^{11, 33, 47, 48}

By including the DFT-D2 or the DFT-D3 contribution due to weak long-range interactions, some of the vibrational modes are sensibly shifted. With respect to the experimental infrared/Raman data,^{44, 45, 49} the results here calculated with dispersion-corrected Hamiltonians are in better agreement with the experimental results, with the lowest MAD s for the PBE-D3 (17.6 cm^{-1}) and B3LYP-D* (5.0 cm^{-1}) approaches. Conversely, both correction schemes increase the mean absolute deviations for PBE0 (21.6 cm^{-1} and 20.2 cm^{-1} for PBE0-D2 and PBE0-D3, respectively), which is probably due to the smaller unit cell, hence, increased bond strengths. Generally, the modes are shifted to higher wavenumbers, with some exception in the low-frequency region. It is interesting noting that the lowest E_u and A_{2u} modes, whose frequency is overestimated by each functional not corrected for van der Waals interactions, are more in line with the experiments when the long-range interactions are properly accounted for.

Table 3. Vibrational frequencies (ν , in cm^{-1}) of calcite as obtained from different DFT Hamiltonians and corrections for weak van der Waals interactions, subdivided according to their irreducible representations (IRREP). Infrared-active modes are reported in two lines, the first related to transverse optical (TO) frequencies, the second to longitudinal optical (LO) ones. Δ_{max} and Δ_{min} are the maximum and minimum differences, respectively, between the theoretical results and the experimental ones, MD is the mean deviation and MAD is the mean absolute deviation.

	IRREP	PBE	PBE-D2	PBE-D3	B3LYP	B3LYP-D*	B3LYP-D3	PBE0	PBE0-D2	PBE0-D3	Exp ⁴⁹
Infrared	E_u	100	77	89	119	105	103	107	87	97	102
		118	101	110	134	124	123	126	110	119	123
	A_{2u}	113	85	101	125	103	103	115	88	103	92
		148	129	141	159	146	147	153	135	146	136
	E_u	212	223	223	219	225	240	223	236	234	223
		224	236	236	230	238	253	235	248	247	239
	E_u	277	298	296	284	300	318	293	315	312	297
		371	388	385	379	390	405	387	405	401	381
	A_{2u}	295	318	317	299	317	337	310	333	331	303
		402	420	418	405	417	432	414	433	430	387
	E_u	684	688	689	711	714	719	719	723	723	712
		686	690	691	712	716	721	721	725	726	715
	A_{2u}	833	832	832	874	875	873	885	884	884	872
		848	848	849	895	896	895	905	905	905	890
	E_u	1358	1372	1368	1398	1408	1415	1445	1458	1454	1407
		1507	1522	1518	1556	1567	1576	1602	1617	1613	1549
Raman	E_g	149	152	154	155	162	165	155	160	161	156
	E_g	268	280	280	275	287	297	280	292	292	284
	E_g	684	687	688	710	713	718	718	722	723	712
	A_{1g}	1051	1060	1059	1085	1093	1099	1111	1119	1119	1086
	E_g	1392	1405	1401	1431	1443	1451	1477	1492	1488	1434
Silent	A_{2g}	184	176	184	191	194	192	187	180	188	
	A_{1u}	286	293	295	289	291	305	295	301	303	
	A_{2g}	309	323	323	312	325	337	317	331	331	
	A_{2g}	837	836	836	881	881	881	892	891	891	
	A_{1u}	1051	1059	1059	1085	1093	1100	1111	1119	1120	
Δ_{max}		21	33	31	33	30	45	52.9	68	63.8	
Δ_{min}		-49	-42	-41	-13	-1	0	-4.21	-15	-4.77	
MD		-18.1	-13.8	-12.1	2.6	6.6	13.8	13.4	18.4	19.4	
MAD		22.7	19.1	18.1	8.4	6.7	13.8	14.7	21.6	20.2	

This suggests that, besides the thermal effects (*i.e.*, lattice expansion) suggested by Valenzano and co-workers,¹¹ these modes are highly sensible to the interactions between the Ca^{2+} and CO_3^{2-} layers (and hence on the c lattice parameter). Indeed, both modes have a displacement component of oxygen atoms along the [001] direction. However, as also suggested by the cited authors, it is strongly necessary to repeat the measurements of infrared and Raman spectra of calcite at low temperatures, to clarify the origin of the deviation of the computing model with respect to the experimental world (limitations in the computational approach and/or in the instrumentation). The infrared absorbance was obtained from the following expression and then used to calculate the spectrum (Figures 3a-c):

$$A(\nu) = \frac{1}{3} \sum_{ii=1}^3 \frac{4\pi}{\lambda \rho} \text{Im}[n_{ii}(\nu)]$$

where the summation runs over the $xx = 1$, $yy = 3$ and $zz = 3$ polarization directions (Voigt's notation), $\text{Im}[n_{ii}(\nu)]$ is the imaginary part of the frequency-dependent refractive index, λ is the wavelength of the incident beam and ρ is the mineral density.^{36, 50, 51} The Raman spectra were computed considering calcite as a polycrystalline powdered specimen, and those reported in Figures 3d-f are related to a parallel polarization. The spectra were calculated using the transverse optical frequencies and the Raman intensities obtained according to the works of Maschio and collaborators,^{52, 53} where each vibrational mode is represented by a pseudo-Voigt function.

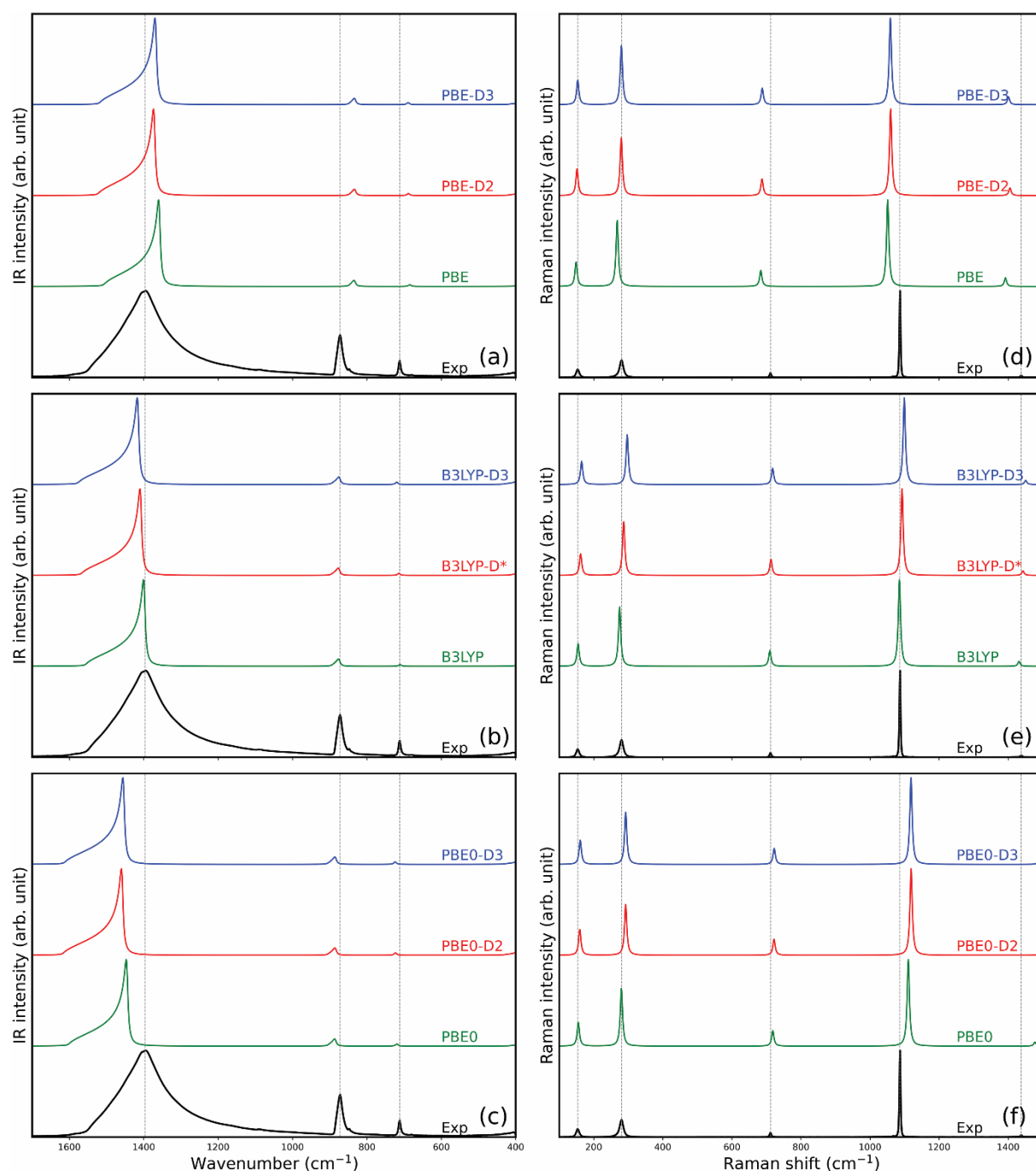


Figure 3. (a-c) Infrared and (d-f) Raman spectra of calcite simulated with different theoretical approaches and compared to experimental data. Experimental infrared and Raman data were taken from the works of Balan et al.⁴⁴ and Rutt and Nicola,⁴⁵ respectively

As a final note, the present work considered two well-known *a posteriori* corrections (DFT-D2 and DFT-D3) to include the effects of long-range interactions in the physical treatment of calcite. DFT-D2 and DFT-D3, together with the DFT-TS approach proposed by Tkatchenko and Scheffler,⁵⁴ are semiempirical *a posteriori* methods that add an attractive term to the DFT total energy of the system. However, it is worth to be mentioned that DFT functionals that explicitly include the long-range interactions in the correlation term have been developed during the past years. An example is given by the vdW-DF non-local correlation functional proposed by Dion et al.⁵⁵ and the

revised vdW-DF2 kernel of Lee co-workers.⁵⁶ In these less empirical approaches, the exchange-correlation energy E_{xc} is expressed as

$$E_{xc} = E_x^{GGA} + E_c^{LDA} + E_c^{nl}$$

where E_x^{GGA} and E_c^{LDA} are the GGA exchange and LDA correlation energies, respectively, and the E_c^{nl} is the non-local correlation energy that is responsible for the van der Waals effects. It was shown that vdW-DF and vdW-DF2 provide more accurate results regarding the structural and elastic properties of different materials.^{57, 58} However, a

Conclusions

Calcite (CaCO_3 , space group $R\bar{3}c$) is an idoneous and adequate platform for benchmarking theoretical methods, such as DFT simulations. Calcite was selected as test crystalline material because its anisotropic structural, electronic, dielectric, optical and vibrational properties are well known and exploited in various and different research and applicative fields, such as chemistry, mineralogy, petrology, optics, and microelectronics. The results here reported highlight the relevancy of the specific *ab initio* approach and related choice of computational parameters:

- with respect to previous DFT simulations,^{10, 11} the inclusion of dispersive forces seems playing an important role in determining the interactions between the alternated layers of Ca^{2+} and CO_3^{2-} (along the [001] direction), affecting the *c* lattice parameter;
- as expectable from previous literature,^{33, 46, 48} hybrid functionals (PBE0 and B3LYP) are best suited for determining the structural and vibrational properties of calcite, albeit the DFT-D3 scheme with the Becke-Johnson damping function seems overestimating the long-range interactions, with too small unit cell and large shifts of vibrational peaks. Instead, the *ad hoc* B3LYP-D* parametrization produced results more in line with the experimental data;
- it is worth stressing that some of these discrepancies are related to the lack of any thermal contribution to the crystal lattice and, consequently, to the other computed properties. A suitable treatment to include temperature effects, for example the quasi-harmonic approximation, could greatly ameliorate the comparison between the theoretical and experimental results.

This study also shows the usefulness of this kind of approach to obtain consistent and possibly predictive results for both known materials and those that could be predicted and developed by adequately calibrated *ab initio* techniques.

Conflicts of interest

There are no conflicts of interest to declare.

References

1. M. Ukita, K. Toyoura, A. Nakamura and K. Matsunaga, *Journal of Applied Physics*, 2016, **120**.
2. A. L. Boettcher and P. J. Wyllie, *The Journal of Geology*, 1968, **76**, 314-330.
3. R. J. Reeder, *Rev. Mineral.*, 1983, **11**, 1-47.
4. M. E. J. Friese, T. A. Nieminen, N. R. Heckenberg and H. Rubinsztein-Dunlop, *Nature*, 1998, **394**, 348-350.
5. C. M. Herne, F. E. Lyons, E. J. Galvez and A. Sam, *Proceedings of SPIE - The International Society for Optical Engineering*, 2020.
6. R. A. Beth, *Physical Review*, 1936, **50**, 115-125.
7. M. Catti, A. Pavese, E. Aprà and C. Roetti, *Physics and Chemistry of Minerals*, 1993, **20**, 104-110.
8. M. Catti, A. Pavese and G. D. Price, *Physics and Chemistry of Minerals*, 1993, **19**, 472-479.
9. A. Pavese, M. Catti, S. C. Parker and A. Wall, *Physics and Chemistry of Minerals*, 1996, **23**, 89-93.
10. M. Prencipe, F. Pascale, C. M. Zicovich-Wilson, V. R. Saunders, R. Orlando and R. Dovesi, *Physics and Chemistry of Minerals*, 2004, **31**, 559-564.
11. L. Valenzano, F. J. Torres, D. Klaus, F. Pascale, C. M. Zicovich-Wilson and R. Dovesi, *Z Phys Chem*, 2006, **220**, 893-912.
12. E. N. Maslen, V. A. Streltsov and N. R. Streltsova, *Acta Crystallogr B*, 1993, **49**, 636-641.
13. R. Dovesi, A. Erba, R. Orlando, C. M. Zicovich-Wilson, B. Civalleri, L. Maschio, M. Rerat, S. Casassa, J. Baima, S. Salustro and B. Kirtman, *Wires Comput Mol Sci*, 2018, **8**, E1360.
14. J. P. Perdew, K. Burke and M. Ernzerhof, *Physical Review Letters*, 1996, **77**, 3865-3868.
15. A. D. Becke, *Journal of Chemical Physics*, 1993, **98**, 5648-5652.
16. A. D. Becke, *Journal of Chemical Physics*, 1993, **98**, 1372-1377.
17. C. T. Lee, W. T. Yang and R. G. Parr, *Physical Review B*, 1988, **37**, 785-789.
18. C. Adamo and V. Barone, *Journal of Chemical Physics*, 1999, **110**, 6158-6170.
19. H. J. Monkhorst and J. D. Pack, *Physical Review B*, 1976, **8**, 5188-5192.
20. S. Grimme, *Journal of Computational Chemistry*, 2006, **27**, 1787-1799.
21. S. Grimme, S. Ehrlich and L. Goerigk, *Journal of Computational Chemistry*, 2011, **32**, 1456-1465.
22. S. Grimme, J. Antony, S. Ehrlich and H. Krieg, *Journal of Chemical Physics*, 2010, **132**, 154104.
23. A. D. Becke and E. R. Johnson, *Journal of Chemical Physics*, 2005, **123**.
24. E. R. Johnson and A. D. Becke, *Journal of Chemical Physics*, 2005, **123**.
25. E. R. Johnson and A. D. Becke, *Journal of Chemical Physics*, 2006, **124**.
26. L. Valenzano, Y. Noel, R. Orlando, C. M. Zicovich-Wilson, M. Ferrero and R. Dovesi, *Theor Chem Acc*, 2007, **117**, 991-1000.
27. G. Ulían and G. Valdrè, *International Journal of Quantum Chemistry*, 2018, **118**, e25553.
28. G. Ulían and G. Valdrè, *International Journal of Quantum Chemistry*, 2018, **118**.
29. G. Ulían and G. Valdrè, *Journal of the Mechanical Behavior of Biomedical Materials*, 2018, **77**, 683-692.
30. D. Moro, G. Ulían and G. Valdrè, *Applied Clay Science*, 2019, **172**, 28-39.
31. D. Moro, G. Ulían and G. Valdrè, *J. Microsc.*, 2020, **280**, 204-221.
32. D. Moro, G. Ulían and G. Valdrè, *Applied Clay Science*, 2020, **197**.
33. F. Pascale, C. M. Zicovich-Wilson, F. L. Gejo, B. Civalleri, R. Orlando and R. Dovesi, *Journal of Computational Chemistry*, 2004, **25**, 888-897.
34. Y. Wang, J. J. Wang, W. Y. Wang, Z. G. Mei, S. L. Shang, L. Q. Chen and Z. K. Liu, *Journal of Physics-Condensed Matter*, 2010, **22**.
35. R. Orlando, V. Lacivita, R. Bast and K. Ruud, *Journal of Chemical Physics*, 2010, **132**, 244106.
36. L. Maschio, B. Kirtman, R. Orlando and M. Rerat, *Journal of Chemical Physics*, 2012, **137**, 204113.
37. L. Maschio, B. Kirtman, M. Rerat, R. Orlando and R. Dovesi, *Journal of Chemical Physics*, 2013, **139**, 164101.

38. S. A. T. Redfern and R. J. Angel, *Contr. Mineral. and Petrol.*, 1999, **134**, 102-106.
39. D. R. Baer and D. L. Blanchard, *Appl Surf Sci*, 1993, **72**, 295-300.
40. D. R. Lide, *CRC Handbook of Chemistry and Physics*, CRC Press Inc., USA, 85th edn., 2004.
41. J. W. Anthony, R. A. Bideaux, K. W. Bladh and M. C. Nichols, *Handbook of Mineralogy. V. Borates, Carbonates, Sulfates*, Mineral Data Publishing, Inc., USA, 2003.
42. F. M. Hossain, G. E. Murch, I. V. Belova and B. D. Turner, *Solid State Communications*, 2009, **149**, 1201-1203.
43. M. G. Brik, *Phys B Condens Matter*, 2011, **406**, 1004-1012.
44. E. Balan, J. Aumont, G. D. Saldi, C. Brouder and M. Lazzeri, *Eur J Mineral*, 2019, **31**, 73-81.
45. H. N. Rutt and J. H. Nicola, *Journal of Physics C: Solid State Physics*, 1974, **7**, 4522-4528.
46. S. Tosoni, C. Tuma, J. Sauer, B. Civalleri and P. Uglierio, *Journal of Chemical Physics*, 2007, **127**.
47. F. Pascale, C. M. Zicovich-Wilson, R. Orlando, C. Roetti, P. Uglierio and R. Dovesi, *Journal of Physical Chemistry B*, 2005, **109**, 6146-6152.
48. G. Uljan, S. Tosoni and G. Valdrè, *Journal of Chemical Physics*, 2013, **139**.
49. K. H. Hellwege, W. Lesch, M. Plihal and G. Schaack, *Z. Physik*, 1970, **232**, 61-86.
50. J. C. Decius and R. W. Hexter, *Molecular Vibrations in Crystals*, McGraw-Hill, New York, USA, 1977.
51. C. F. Bohren and D. Huffman, *Absorption and scattering of light by small particles*, Wiley-Interscience Publication, New York, USA, 1983.
52. L. Maschio, B. Kirtman, M. Rerat, R. Orlando and R. Dovesi, *Journal of Chemical Physics*, 2013, **139**, 164102.
53. L. Maschio, B. Kirtman, S. Salustro, C. M. Zicovich-Wilson, R. Orlando and R. Dovesi, *Journal of Physical Chemistry A*, 2013, **117**, 11464-11471.
54. A. Tkatchenko and M. Scheffler, *Physical Review Letters*, 2009, **102**, 073005.
55. M. Dion, H. Rydberg, E. Schröder, D. C. Langreth and B. I. Lundqvist, *Physical Review Letters*, 2004, **92**, 246401.
56. K. Lee, E. D. Murray, L. Z. Kong, B. I. Lundqvist and D. C. Langreth, *Physical Review B*, 2010, **82**, 4.
57. N. V. Ilawe, J. A. Zimmerman and B. M. Wong, *Journal of Chemical Theory and Computation*, 2015, **11**, 5426-5435.
58. J. H. Lee, J. H. Park and A. Soon, *Physical Review B*, 2016, **94**, 11.